Journal of Solid State Chemistry 186 (2012) 255–260

Contents lists available at SciVerse ScienceDirect

Journal of Solid State Chemistry

journal homepage: www.elsevier.com/locate/jssc

Large-scale controllable synthesis of dumbbell-like $BiVO_4$ photocatalysts with enhanced visible-light photocatalytic activity

Yang Lu [a,b], Yong-Song Luo [a,b,*], De-Zhi Kong [a], De-Yang Zhang [a], Yong-Lei Jia [a], Xin-Wei Zhang [a]

[a] Department of Physics & Electronic Engineering, Xinyang Normal University, Xinyang 464000, China
[b] Technical Institute of Physics and Chemistry, Chinese Academy of Sciences, Beijing 100190, China

ARTICLE INFO

Article history:
Received 13 September 2011
Received in revised form
1 December 2011
Accepted 2 December 2011
Available online 17 December 2011

Keywords:
Controllable synthesis
Bismuth vanadate
Hydrothermal
Photocatalytic

ABSTRACT

The controllable synthesis of novel dumbbell-like $BiVO_4$ hierarchical nanostructures has been successfully obtained via a simple hydrothermal route. The as-synthesized products were studied by X-ray powder diffraction, scanning electron microscopy, transmission electron microscopy and UV–vis absorption spectroscopy. The results showed that the nucleation and growth of the nanodumbbells were governed by an oriented aggregation growth mechanism. It is noteworthy that the concentration of poly(vinyl pyrrolidone) and the volume ratio of H_2O to CH_3COOH were crucial to the growth of the final nanoarchitectures. Control experiments were also carried out to investigate the factors which impact on the morphology of the products. Furthermore, the as-prepared $BiVO_4$ hierarchical nanostructures demonstrated the superior visible-light-driven photocatalytic efficiency, which is helpful for the separation and recycle considering their promising applications in harmful pollutants disposal.

1. Introduction

Hierarchical self-assembly of nanosized building blocks, including nanowires, nanobelts, nanoplatelets, nanotubes, nanorods, etc. has been a focus of recent interest in material science owing to these parameters represents key elements that determine their properties and applications [1–5]. Thus, fabricating complex architectures, especially highly ordered three-dimensional (3D) superstructures, brings about a lot of new properties and applications to functional materials [6–9]. In this field, the dumbbell structure, which is existing example of common architecture in nature, has attracted considerable attention recently. For example, room-temperature template-free synthesis of dumbbell-like $SrSO_4$ with hierarchical architecture [10], and growth and dissolving mechanism of dumbbell-like ZnO bipod crystal [11]. However, the synthesis of dumbbell-like hierarchical nanostructures is not nearly enough so far. Therefore, a challenge remains for material scientists to find simple and reliable methods for the controlled synthesis dumbbell-like hierarchical nanostructures with designed chemical components and expected functionalities.

$BiVO_4$, with a 2.4 eV bandgap, exists in three phase: monoclinic scheelite, tetragonal zircon, and tetragonal scheelite [12]. It is accepted that $BiVO_4$ is an important semiconductor owing to its excellent properties such as ferroelasticity [13], acousto-optical [14], ionic conductivity [15], etc. This compound has a wide range of applications in pigments, ionic conductivity [15] and ferroelasticity [16], also has the ability to photodegrade organic pollutants under visible-light irradiation [17]. Recently, many fabrications of crystalline $BiVO_4$ methods were reported, such as solid-state [18–21], aqueous [22,23], and hydrothermal processes [24–26]. For example, Zhou et al. [7] controlled synthesis of three-dimensional well-defined $BiVO_4$ mesocrystals via a facile additive-free aqueous strategy. Kudo et al. [27] selectively synthesized monoclinic and tetragonal zircon $BiVO_4$ at room temperature in aqueous solution by reactions of layered potassium vanadates with $Bi(NO_3)_3$. Zhao et al. [28] reported the surfactant-free synthesis of hyperbranched monoclinic $BiVO_4$ and its applications in photocatalysis, gas sensing, and lithium-ion batteries. In generally, hydrothermal method exhibits many strong points over other conventional methods. The benefits of this method are the relatively mild synthesis conditions, high degree of crystallinity, high purity, and narrow particle size distribution of product.

Herein, we demonstrate a facile method for the control synthesis of a novel $BiVO_4$ hierarchical nanostructure. Dumbbell-like $BiVO_4$ hierarchical nanostructures has been synthesized by the hydrothermal treatment of $Bi(NO_3)_3 \cdot 5H_2O$ and NH_4VO_3 under acidic conditions. The morphology evolution and the growth mechanisms were investigated carefully. As an important metal oxide semiconductor with hierarchical nanostructures, we also evaluated the photocatalytic activity of the $BiVO_4$ nanodumbbells

* Corresponding author at: Department of Physics & Electronic Engineering, Xinyang Normal University, Xinyang 464000, China. Fax: +86 376 6391705.
E-mail addresses: ysluo@mail.ipc.ac.cn, ysluo@mail2.xytc.edu.cn (Y.-S. Luo).

0022-4596/$ - see front matter © 2011 Elsevier Inc. All rights reserved.
doi:10.1016/j.jssc.2011.12.003

for applications in photodegradation of rhodamine B(RhB) under visible-light irradiation, which indicates that dumbbell-like $BiVO_4$ represents an advanced material for photocatalyst with predictable functionalities.

2. Experimental

All the chemicals were of analytical grade reagent and employed without further purification. Dumbbell-like $BiVO_4$ nanostructures were obtained as follows: 1 mmol NH_4VO_3 was dissolved in 15 ml of H_2O:CH_3COOH mixed solution with a volume ratio of 2:1 and the obtained solution was sonicated in an ultrasonic water bath for 30 min, the prepared solution is marked as solution A. At the same time, 1 mmol $Bi(NO_3)_3 \cdot 5H_2O$ and 0.5 g of poly(vinyl pyrrolidone) (PVP) were also dissolved in the 15 ml H_2O:CH_3COOH mixed solution with a volume ratio of 2:1 by vigorous stirring, and the resultant solution is marked as solution B. When the solutions A and B were dissolved adequately, two solutions were mixed and the obtained mixture was stirred for 20 min until it became homogeneous. Then the prepared solution was sealed in a Teflon-lined stainless steel autoclave. And the autoclave was sustained at 180 °C for 15 h, and then was cooled to room temperature naturally. Finally, the products were separated from solution by centrifugation, washed times with ethanol and distilled water to remove any ionic residual then dried in oven at 60 °C for 10 h for further characterization. In order to compare the products, other morphological products were also prepared with different experimental parameter.

The phase purity of the products was characterized by X-ray powder diffraction (XRD) using a D8 Focus (Germany, Bruker) automated X-ray diffractometer system with Cu-$K\alpha$ radiation (λ=1.5418 Å). Scanning electron microscopy (SEM) images and X-ray energy dispersive spectroscopy (EDS) analyses were obtained using a HITACHI S-4300 microscope (Japan). Transmission electron microscopy (TEM) and high-resolution transmission electron microscopy (HRTEM) images and the corresponding selected area electron diffraction (SAED) patterns were obtained on a JEOLJEM-2010 instrument in bright field and an HRTEMJEM-2010FEF instrument (operated at 200 kV), respectively. The room-temperature UV–vis absorption spectrum was recorded on a TU-1901 spectrophotometer in wavelength range of 200–800 nm.

Photocatalytic activities of the obtained products were evaluated by the degradation of RhB under visible light irradiation using a 500 W Xe lamp with a cut-off filter ($\lambda > 400$) nm. In each experiment, 0.3 g of the photocatalyst was added to 600 ml of RhB solution (10^{-5} mol L^{-1}). Before illumination, stirred the solution slightly in the dark for 1 h to insure the formation of an adsorption–desorption equilibrium between the photocatalyst and RhB. And then the solution was exposed to visible light irradiation and bubbled with an air pump to provide enough oxygen. At regular time intervals, a 10 ml solution was sampled and centrifuged to remove the residual photocatalyst. Finally, the adsorption UV–vis spectra were recorded on a TU-1901 spectrophotometer.

3. Results and discussion

Dumbbell-like $BiVO_4$ nanoarchitectures were synthesized by the reaction between Bi^{3+} and VO_3^- ions in a H_2O/CH_3COOH solution system at the appropriate temperature of 180 °C. Fig. 1a–c shows the SEM images of the dumbbell-like $BiVO_4$ sample at low, medium and high magnification, respectively. According to the SEM observations, it displays that the as-prepared $BiVO_4$ product is composed of countless dumbbell-like aggregates, single dumbbells have a length ranging from 2 to 5 μm, and nearly all of them hold the same morphology (Fig. 1a and b). Furthermore, we can notice that the surface of the obtained $BiVO_4$ sample is fairly rough as shown in Fig. 1c, which further indicates that every dumbbell is composed of plenty nanoparticles. Fig. 1d shows a typical XRD pattern of the obtained dumbbell-like $BiVO_4$ sample. All of the diffraction peaks are identical to the standard Joint Committee on Powder Diffraction Standards (JCPDS) card No. 14-0688. No peaks for other phases or impurities were observed, which demonstrated the high purity of the prepared product. These results show that

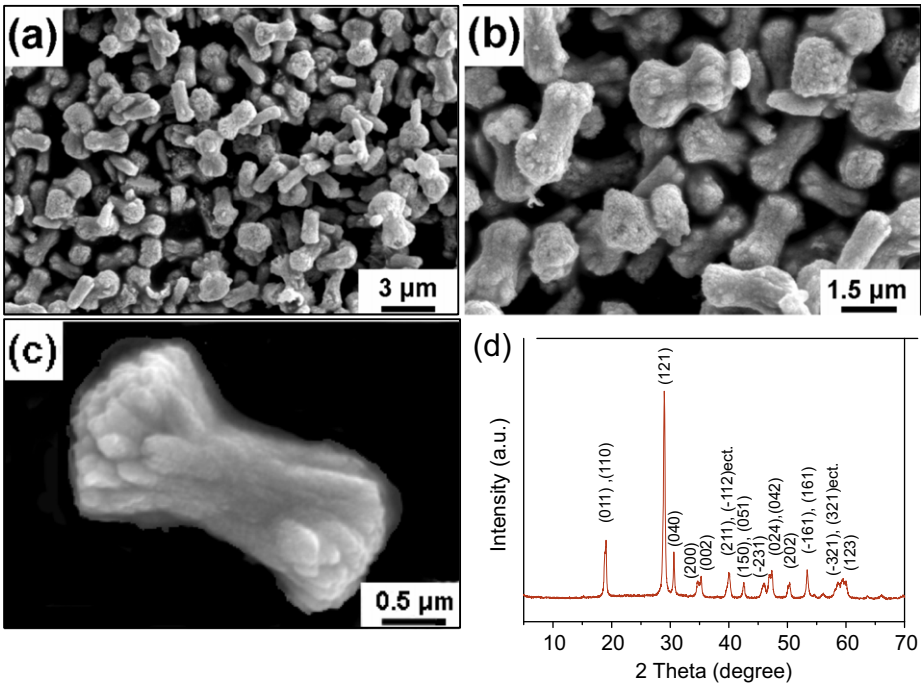

Fig. 1. (a) Low-magnification SEM image of the as-prepared $BiVO_4$ dumbbells; (b) enlarged SEM image of the $BiVO_4$ dumbbells; (c) SEM image of an individual $BiVO_4$ dumbbell; (d) powder XRD pattern of the as-prepared $BiVO_4$ dumbbells.

the adopted hydrothermal route is well-disposed to the formation of polycrystalline $BiVO_4$.

In order to get more information about the microstructure of as-prepared dumbbell-like products, the further investigation is performed by TEM and HRTEM. Fig. 2a and b shows the general and individual magnification TEM images respectively. The related selected area electron diffraction (SAED) pattern of the dumbbell-like $BiVO_4$ is inserted in Fig. 2a, which shows that the obtained $BiVO_4$ products possess polycrystalline structure. A great contrast between the edge and center of the dumbbell can be distinctly noticed (Fig. 2b), further confirming their dumbbell nature. Fig. 2c pictures the typical HRTEM image of the fringe part of a dumbbell, and the inset is enlarged image of the area marked by a rectangle, which reveals the resolved lattice spacing of 0.257 nm. The as-obtained samples were also predicated by EDS analysis. The EDS result displayed in Fig. 2d demonstrates that the products are composed of Bi, V, O, and Pt. The Pt-element is induced by the spattering Pt nanoparticles used for the SEM samples. According to the quantitative EDS analysis, the atomic ratio of Bi, V, and O is nearly 1:1:4, which match to the standard stoichiometric composition.

To further understand the morphological evolution, time-dependent experiments were carried out by extracting products at different reaction stages. The morphological evolutions of the intermediate products were carefully recorded by SEM as shown in Fig. 3. The detailed morphological evolution process of the $BiVO_4$ products can be described as follows. Fig. 3a shows that lots of tiny particles were assembled before being transferred to the Teflon-sealed autoclave. After hydrothermal reaction for 1 h, the resultant products are irregular nano- and micro-sized particles and the surfaces of these particles is coarse (Fig. 3b). When the reaction was prolonged to 3 h, a few rod-like $BiVO_4$ nanoarchitectures exist in the products as shown in Fig. 3c. As the reaction proceeds from 9 h to 12 h, lots of ill-defined dumbbell-like architectures were produced (Fig. 3d and e). On gradual evolution of the $BiVO_4$ nanostructures, well-defined nanodumbbells are obtained after a reaction time of 15 h, most of the obtained products are uniform dumbbells as shown in Fig. 3f, and almost no impurities can be observed.

It is noted that the oriented aggregate mechanism [29] has been proposed to account for the formation of dumbbell-like $BiVO_4$ nanoarchitectures successfully. First, when the reaction was performed in the solution-phase system before being transferred to the Teflon-sealed autoclave, it directly gave fine $BiVO_4$ particles, which were formed in the solution through a homogeneous nucleation process, the small $BiVO_4$ particles grow to large particles via a process known as Ostwald ripening [30], as the aging process continues. Second, when the reaction was carried out at 180 °C for 1 h, partial $BiVO_4$ nanoparticles start to dissolve into the solution and further grow into the sphere-like nanocrystals through recrystallization. After a longer aging time, the sphere-like products gradually grow larger rod-like structures by oriented aggregation process. Finally, the rod-like nanocrystals gradually evolve to 3D dumbbell-like nanostructures through continuous aggregation attachment. Moreover, in this experiment, PVP plays a key role in the formation of the as-synthesized products. As is well known, using PVP as a capping agent, which has been widely prepared [31–33]. For example, Giuffrida et al. have reported that PVP is presumably complexed with $Cu(acac)_2^+$ to form a $Cu(acac)_2^+$–PVP intermediate during the photochemical synthesis of Cu NPs [34]. This means that the pyrrole moiety of PVP might be negatively charged, and thus, coordinates a positive ion. In our system, the PVP is used as a "soft" template. We speculate that during addition of an amount of PVP to the reaction solution, many active sites will be produced around the circumference of $BiVO_4$ nuclei (the $BiVO_4$ nanoparticles formed earlier) in the hydrothermal conditions. In addition, The existence of Bi^{3+} ions in our reaction system can be naturally understood as the formation of the Bi^{3+}–PVP complex or $BiVO_4$–PVP NPs in the solution. These combinations begin to self-assemble and further change into a dumbbell aggregated structure. Herein, we propose that PVP is to kinetically control the growth rates of the different crystalline planes through the selective interaction in the adsorption and desorption processes. Moreover, the process of the shape

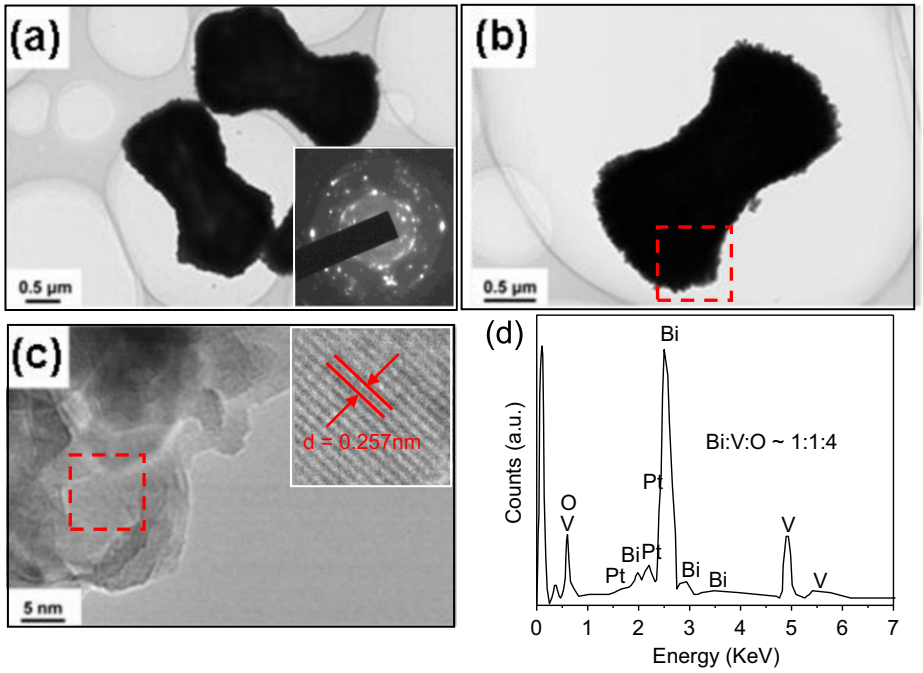

Fig. 2. (a) TEM image of the as-prepared $BiVO_4$ dumbbells and the inset is the SAED result of the products; (b) TEM image of an individual $BiVO_4$ dumbbell; (c) HRTEM image of the fringe part of a dumbbell (inset is enlarged image of the area marked by a rectangle); (d) EDS result of the as-synthesized $BiVO_4$ dumbbells.

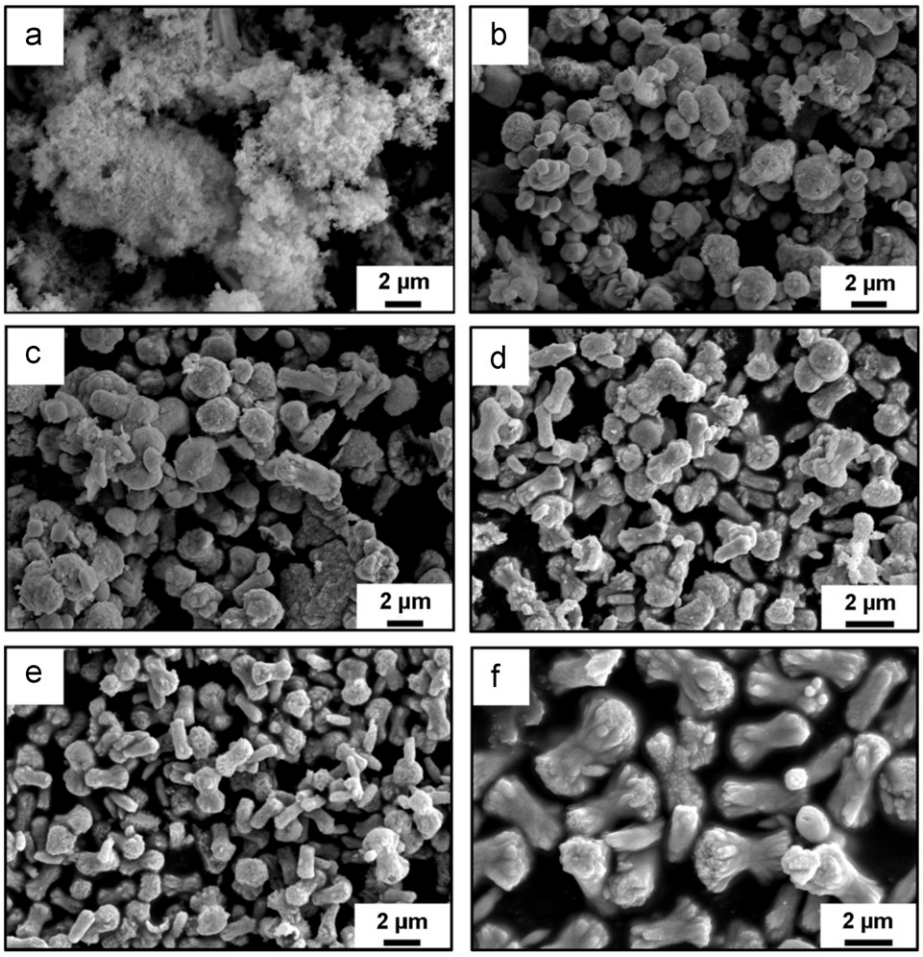

Fig. 3. Time-dependent morphological evolution of the $BiVO_4$ products at different growth stages: (a) 0 h, (b) 1 h, (c) 3 h, (d) 9 h, (e) 12 h, and (f) 15 h.

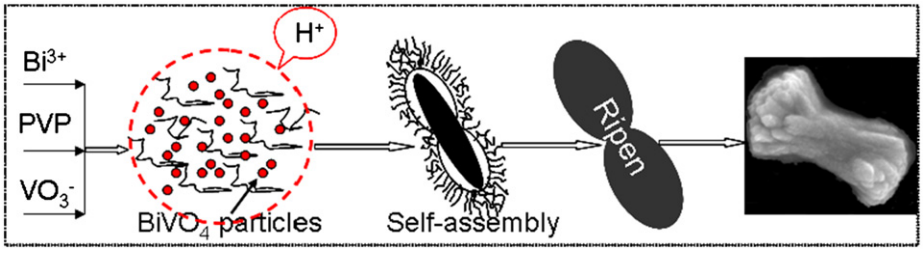

Fig. 4. Schematic illustration of the proposed formation mechanism of dumbbells $BiVO_4$ hierarchical nanostructures.

transition from nanoparticles, nanorods to nanodumbbells is also summarized in Fig. 4.

Control experiment study was also demonstrated that the final morphologies of the as-prepared products are strongly affected by different reactive conditions. When added amount of CTAB (0.5 g or 1.0 g), the resultant products is plate-like or bowl-like $BiVO_4$ nanostructures as revealed by the SEM images (Fig. 5a and b). In addition, the concentration of PVP in the solution also affects the morphology of the $BiVO_4$ products. Fig. 5c displays a completely different kind of $BiVO_4$ morphology in the absence of PVP. Moreover, Fig. 5 also shows the SEM images of the as-synthesized products obtained at the different values of ω (the volume ratio of H_2O to CH_3COOH), respectively. It is clear that the morphology of the products critically depends on this volume ratio. For ω=1:2, the nanoclews appear in our obtained products, which with size of 3–7 μm (Fig. 5d). When the ω value is increased to 1:1, some nanoclews and nanodumbbells nanostructures are observed in the products (Fig. 5e). When the ω value is increased to 2:1, we can observe that the uniform dumbbell-like $BiVO_4$ nanostructures were obtained (Fig. 5f).

The optical property of dumbbell-like $BiVO_4$ nanostructures was investigated by UV/Vis diffuse reflectance spectrum. The result is shown in Fig. 6a. As can be seen, there is a broad peak in the range of 300–450 nm, shows a strong absorption in the visible-light region in addition to that in the UV-light region. According to the equation $\alpha E_p = K(E_p - E_g)^{1/2}$ (where α is the absorption coefficient, K is a constant, E_p is the discrete photo energy, and E_g is the bandgap energy) [35], a classical Tauc approach is further employed to estimate the E_g value of dumbbell-like $BiVO_4$ nanostructures. The plot of $(\alpha E_p)^2$ versus E_p based on the direct transition is shown in the inset of Fig. 6. The extrapolated value (the straight lines to the X axis) of E_p at α=0 gives absorption edge energies corresponding to E_g=2.51 eV, which is consistent with previous reports [36].

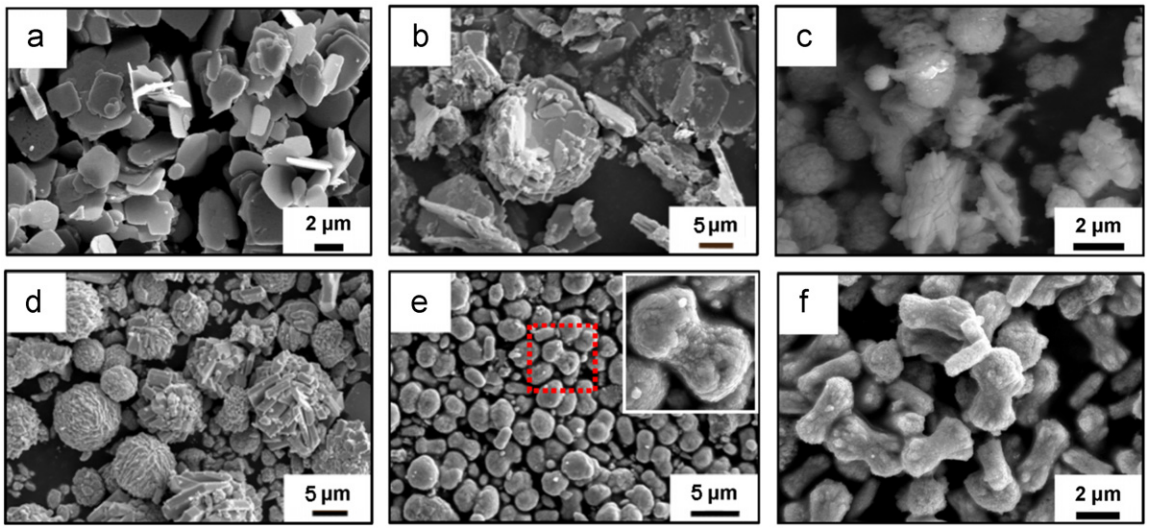

Fig. 5. Typical SEM images of $BiVO_4$ products obtained at different condition: (a) in the presence of 0.5 g CTAB, (b) in the presence of 1.0 g CTAB, (c) in the absence of PVP; the volume ratios of H_2O/CH_3COOH for (d) 1:2, (e) 1:1, and (f) 2:1.

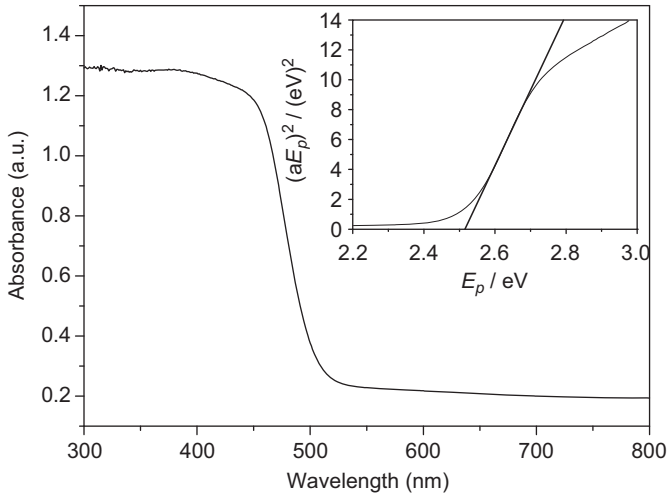

Fig. 6. The UV/vis diffuses reflectance spectra of $BiVO_4$ dumbbells. Inset: a plot of $(\alpha E_p)^2$ versus photon energy (E_p).

The photocatalytic activity of the dumbbell-like $BiVO_4$ nanostructures was evaluated by using the degradation of dye RhB in air and compared with P25 under the same conditions (Fig. 7). Fig. 7a shows the decrease in UV/vis absorption intensity of the solution of RhB with time, recorded at 30 min intervals. We can observe that the photodegradation rate is over 50% after 60 min under visible-light irradiation ($\lambda > 400$ nm), and which demonstrates superior photocatalytic abilities of dumbbell-like $BiVO_4$. From the gradual decrease of RhB absorption under irradiation of visible light at the wavelength of 553 nm, we also discover an absorption band shift to shorter wavelengths. This hypsochromic shift may be attributed to the dye's de-ethylation, that is, from N,N,N,′N′-tetraethylated RhB to RhB [37]. Fig. 7b shows the results of the RhB degradation efficiencies with different conditions under visible-light illumination, the photocatalytic activity of $BiVO_4$ was up to 90% in 4.5 h under visible-light irradiation, it is obvious that dumbbell-like $BiVO_4$ nanostructures exhibits superior photocatalytic abilities over P25(Commercial Degussa P25 TiO_2). The superior visible-light-driven photocatalytic efficiency

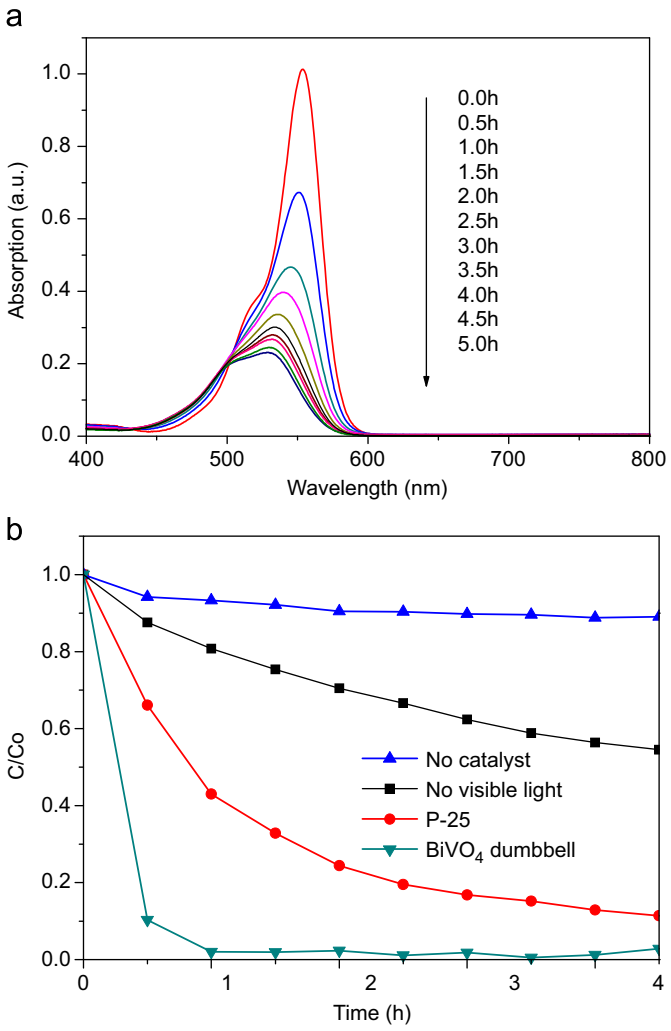

Fig. 7. (a) The temporal evolution of the absorption spectra of the RhB solution in the presence of $BiVO_4$ dumbbells under exposure to visible light; (b) the effect of different catalysts and different conditions on photocatalytic degradation of RhB (initial concentration 1.0×10^{-5} M).

of dumbbell-like $BiVO_4$ could be attributed to its loosely packed mesoporous nanostructure, which is very benefit to absorb the abundant RhB molecules, meanwhile, exposing many crystal planes could not only provide more active sites for the photocatalytic reaction but also effectively promote the separation efficiency of the electron-hole pairs. Therefore, these will accelerate the degradation of RhB solution.

4. Conclusions

In conclusion, well-defined dumbbell-like $BiVO_4$ hierarchical nanostructures have been obtained under a reaction temperature of 180 °C for 15 h at a proper volume ratio of H_2O:CH_3COOH=2:1. Experimental results indicated that the morphologies of as-synthesized $BiVO_4$ were strongly affected by the concentration of PVP and the volume ratio of H_2O to CH_3COOH. Furthermore, the as-prepared $BiVO_4$ hierarchical nanostructures demonstrate the superior visible-light-driven photocatalytic efficiency, which is helpful for the separation and recycle considering their promising applications in harmful pollutants disposal.

Acknowledgments

The authors acknowledge the China Postdoctoral Key Science Foundation, and the Science and Technology Planning Project of He'nan Province of China (112102310565).

References

[1] M. Shang, W.Z. Wang, J. Ren, S.M. Sun, L. Zhang, CrystEngComm. 12 (2010) 1754.
[2] X.J. Dai, Y.S. Luo, S.Y. Fu, W.Q. Chen, Y. Lu, Solid State Sci. 12 (2010) 637.
[3] S. Sun, C.B. Murray, D. Weller, L. Folks, A. Moser, Science 287 (2000) 1989.
[4] S.B. Sun, X.T. Chang, L.H. Dong, Y.D. Zhang, Z.J. Li, Y.Y. Qiu, J. Solid State Chem. 184 (2011) 2190.
[5] X.S. Fang, Y. Bando, M.Y. Liao, U.K. Gautam, C.Y. Zhi, B. Dierre, B.D. Liu, T.Y. Zhai, T. Sekiguchi, Y. Koide, D. Golberg, Adv. Mater. 21 (2009) 2034.
[6] Y.P. Yuan, J.T. Zai, Y.Z. Su, X.F. Qian, J. Solid State Chem. 184 (2011) 1227.
[7] L. Zhou, W.Z. Wang, H.L. Xu, Cryst. Growth Des. 8 (2008) 728.
[8] X.S. Fang, C.H. Ye, L.D. Zhang, J.X. Zhang, J.W. Zhao, P. Yan, Small 1 (2005) 422.
[9] Y.S. Luo, S.Q. Li, Q.F. Ren, J.P. Liu, L.L. Xing, Y. Wang, Y. Yu, Z.J. Jia, J.L. Li, Cryst. Growth Des. 7 (2007) 87.
[10] Y.F. Li, J.H. Yang, Y. Zhou, X.S. Liang, T. Murakami, S. Sasaki, J. Cryst. Growth 312 (2010) 1886.
[11] E.S. Jang, J.H.W.,.Y.W. Kim, Z. Cheng, J.H. Choy, CrystEngComm. 13 (2011) 546.
[12] J.D. Bierlein, A.W. Sleight, Solid State Commun. 16 (1975) 69.
[13] W.I.F. David, I.G. Wood, J. Phys. C: Solid State Phys. 16 (1983) 5149.
[14] C. Manolikas, S. Amelinckx, Phys. Status Solidi A 60 (1980) 167.
[15] K. Hirota, G. Komatsu, M. Yamashita, H. Takemura, O. Yamaguchi, Mater. Res. Bull. 27 (1992) 823.
[16] Y.T. Yeom, S.H. Choh, M.L. Du, M.S. Jang, Phys. Rev. B 53 (1996) 3415.
[17] S. Kohtani, M. Koshiko, A. Kudo, K. Tokumura, Y. Ishigaki, A. Toriba, K. Hayakawa, R. Nakagaki, Appl. Catal. B: Environ. 46 (2003) 573.
[18] A. Kudo, K. Ueda, H. Kato, I. Mikami, Catal. Lett. 53 (1998) 229.
[19] R.S. Roth, J.L. Waring, Am. Mineral. 48 (1963) 1348.
[20] A.W. Sleight, H.Y. Chen, A. Ferretti, D.E. Cox, Mater. Res. Bull. 14 (1979) 1571.
[21] A.R. Lim, S.H. Choh, M.S. Jang, Condens. Matter. 7 (1995) 7309.
[22] A. Kudo, K. Omori, H. Kato, Am. Chem. Soc. 121 (1999) 11459.
[23] S. Tokunaga, H. Kato, A. Kudo, Chem. Mater. 13 (2001) 4624.
[24] L. Zhang, D.R. Chen, X.L. Jiao, J. Phys. Chem. B 110 (2006) 2668.
[25] J.Q. Yu, A. Kudo, Adv. Funct. Mater. 16 (2006) 2163.
[26] J. Liu, H. Wang, S. Wang, H. Yan, Mater. Sci. Eng. 104 (2003) 36.
[27] A. Kudo, K. Omori, H. Kato, J. Am. Chem. Soc. 121 (1999) 11459.
[28] Y. Zhao, Y. Xie, X. Zhu, S. Yan, S.X. Wang, Chem. Eur. J. 14 (2008) 1601.
[29] Q. Gong, X. Qian, X. Ma, Z. Zhu, Cryst. Growth Des. 6 (2006) 1821.
[30] A.R. Roosen, W.C. Carter, Phys. A 261 (1998) 232.
[31] B.K. Park, S. Jeong, D. Kim, J. Moon, S. Lim, J.S. Kim, J. Colloid Interface Sci. 311 (2007) 417.
[32] H. Zhang, X. Ren, Z. Cui, J. Cryst. Growth 304 (2007) 206.
[33] H. Zhang, Z. Cui, Mater. Res. Bull. 43 (2008) 1583.
[34] S. Giuffrida, L. Costanzo, G. Ventimiglia, C. Bongiorno, J. Nanopart. Res. 10 (2008) 1183.
[35] S. Tsunekawa, T. Fukuda, A. Kasuya, J. Appl. Phys. 87 (2000) 1318.
[36] L. Zhou, W. Wang, S. Liu, L. Zhang, H. Xu, W. Zhu, J. Mol. Catal. A 252 (2006) 120.
[37] X.J. Dai, Y.S. Luo, W.D. Zhang, S.Y. Fu, Dalton Trans. 39 (2010) 5.